Monte Carlo simulations of radial displacement of oil from a wetted porous medium: fractals, viscous fingering and invasion percolation

1988 J. Phys. A: Math. Gen. 21 2979

(http://iopscience.iop.org/0305-4470/21/13/021)

J. Phys. A: Math. Gen. **21** (1988) 2979-2994. Printed in the UK

Monte Carlo simulations of radial displacement of oil from a wetted porous medium: fractals, viscous fingering and invasion percolation

Denys F Leclerc† and Graham H Neale

Department of Chemical Engineering, University of Ottawa, Ottawa, Ontario K1N 6N5, Canada

Received 2 October 1987, in final form 21 March 1988

Abstract. A numerical random-walk method for simulating pore-size radial displacement of oil from wetting porous media under varying conditions of pore-size distribution, wettability, mobility ratio and capillary numbers is described. The algorithm involves Monte Carlo decision making, random walks and percolation theory. The likelihood of having a walker start from a peripheral site, or from the origin, is determined by the viscosity ratio, M. Sticking probabilities, however, depend on the interfacial tension, γ, and the solid-liquid contact angle, θ. Three limiting behaviours are identified in terms of viscosity ratio and capillary number: viscous fingering, plug flow and invasion percolation. Numerical experiments are performed for $M = 13$ ($\gamma = 18$ mN m^{-1}, $\theta = 50°$), and for $M = 7.6 \times 10^{-5}$ ($\gamma = 66$ mN m^{-1}, $\theta = 70°$) at flow rates spanning four decades on a porous network of pores and sites having a log-normal size distribution. Typical runs last about 5-10 min. Preliminary evidence of partially dendritic growth at high capillary number is discussed. Agreement with previously reported experiments is excellent.

List of symbols used

$a_{b;s}$	diameter of bond; site.
$C(R/r, \theta)$	geometric constant due to radial flow.
d	integer dimension (=2 for this work).
D	fractal dimension.
$f(x)$	probability of having k active bonds in a x-neighbour geometry.
F	lattice unit size.
h	porous medium thickness.
k	number of active bonds per site.
L	extent of linear-flow porous media.
m	time (Monte Carlo steps/site).
M	viscosity ratio ($=\mu_{NW}/\mu_W$).
N	number of lattice units occupied by the displacing fluid.
N_{ca}	capillary number.

† Present address: The Pulp and Paper Research Institute of Canada, Vancouver Laboratory, 3800 Wesbrook Mall, Vancouver, BC, V6S 2L9, Canada.

0305-4470/88/132979+16$02.50

p	probability of finding a random walker at site s.
$\delta p_{NW;W}$	intraphase pressure drop: non-wetting; wetting.
p_c	capillary pressure ($=(4\gamma \cos \theta)/a_b$).
∇P	pressure gradient.
q	volumetric flow rate.
r	radial distance (in lattice units).
R	breakthrough radius (in lattice units).
S_{NW}	non-wetting phase saturation.
V	interface velocity (lattice units/walk step).
$\bar{V}$	normalised interface velocity.
γ	interfacial surface tension.
$\Gamma_{W;NW}(s; b)$	evaporation probability; percolation probability.
ε	porosity
θ	solid-liquid contact angle.
κ	permeability.
λ	generic mobility in Darcy's law ($=\kappa/\mu_{NW;W}$).
$\mu_{NW;W}$	bulk phase viscosity: non-wetting; wetting.
$\phi_{NW;W}(b; s)$	sticking probability: non-wetting; wetting.

1. Introduction

Viscous fingering in porous media has been a long-standing problem for researchers trying to understand this phenomenon in order to effect economical oil recovery. Recently, however, a number of advances have been made which suggest that a workable solution will eventually be found. This progress has been reviewed extensively by Witten and Cates [1] concerning disorderly growth processes, and by Homsy [2] on the topic of viscous fingering. These authors give an excellent overview of recent theoretical and experimental developments.

A question that stood unresolved for many years was the origin of finger instability: experimental results [3] could not be accounted for by classical linear stability analysis [4-6]. Either unstable fingers were forecast where only stable fingers were observed [3, 6], or finger thickness could not be reconciled with simulation results [6], even though finger shape was successfully predicted. This unhappy state of affairs changed when boundary integral methods were applied to the problem: numerical experiments by Tryggvason and Aref [7] and by De Gregoria and Schwartz [8] have shown that, if surface tension is properly incorporated in the calculations, stable fingers will develop over a wide range of capillary numbers. Also, those fingers become increasingly unstable with decreasing surface tension, as has been observed experimentally with Hele-Shaw cells.

Meanwhile, an attempt by Paterson [9] at modelling immiscible radial flow displacement in Hele-Shaw cells was extended to porous media by Ni *et al* [10], where displacement of glycerin by parraffin oil was observed to depend on the relative strengths of capillary and viscous forces. Good agreement between theory and experiment was obtained. Lately, investigators [9, 11] have stressed the importance of the capillary number, N_{ca}, as a relevant parameter for predicting finger width, which for wetting media decreases linearly with N_{ca}. Recent porous media simulations confirm this observation by using a pore-site network [12]. Unfortunately, no simulations were

carried out at viscosity ratios other than unity. Therefore, it is very difficult to use these results for predicting finger behaviour at very low viscosity ratios.

1.1. The DLA *model*

In the last few years, there has been a conjecture that, as the capillary number increases to very large values, fingering patterns become fractals, with complex, tree-like structures which are characterised by a single parameter, the fractal dimension, D. The prevailing model used is that of diffusion-limited growth (i.e. aggregation), better known as DLA. Following earlier investigations by Mullins and Sekerka [13] on the aggregation of condensed matter, Forrest and Witten [14] conducted a study of long-range correlations in a two-dimensional cross section taken from a three-dimensional smoke particle aggregate. Their analysis suggested that the aggregation process of such an aerosol was occurring in a self-similar manner and that the fractal dimension of the object was between 1.5 and 1.8. As to the origin of this process, it is now widely accepted that the aggregation of colloids and aerosols is best described by the 'clustering of clusters' model. At the time, however, the discovery of the fractal character of smoke aggregates spurred Witten and Sander [15] to propose a model for their formation. This model is based upon potential theory and serves as the mathematical foundation for the diffusion-limited growth (DLA) model; the most effective way to simulate such a process is to let random walkers wander over an arbitrary lattice and stick on the growing cluster upon first contact. This situation corresponds to a negligible surface tension and the growth rate gives a fractal dimension that agrees well with most observations [16]. Computer simulations by Meakin [17] confirmed those findings. Similar results were obtained by Turkevitch and Scher [18] using a reformulation of DLA that uses occupancy probabilities on the unscreened tips of the aggregate. Examples of diffusion-limited growth include the electrodeposition of zinc metal [19] and the Litchtenberg figures seen in dielectric breakdown [20]. However, the irreversible kinetic aggregation of aqueous gold colloids [21] is now interpreted as a 'clustering of clusters'; this model was introduced by Meakin [22] and by Kolb *et al* [23] and is now the best available explanation for the formation of aerosol structures.

Paterson [24] noted similarities between DLA and two-phase fluid flow in porous media, provided that experimental conditions maximise the capillary number, N_{ca}, and that the displacing fluid is practically inviscid with respect to the displaced fluid; thus, interface instabilities keep growing because they are amplified by the high mobility of the displacing fluid [24]. Experiments in linear [25] and radial [26] Hele-Shaw cells show that viscous fingering at nearly infinite mobility ratios generates fractals with a fractal dimension equal to 1.7 for a radially symmetric cell geometry.

Non-wetting displacement experiments at high N_{ca} in porous media gave essentially the same results [27], except that fingers did not grow beyond pore-level size. The DLA model, however, is simplistic and is limited in scope: it does not address finite mobility ratios, non-zero surface tension or relative permeabilities. Nevertheless, it can account for pore-size distribution: Chan *et al* [28] and Chen and Wilkinson [29] have shown that when pore sizes are exponentially or uniformly distributed over [0, 1], DLA-like patterns will develop. Dendritic fingers are seen only when most pores have the same radius.

A number of approaches have been devised to adapt the DLA model to finite-mobility situations: De Gregoria [30] used an analogy with an electrical network of resistors to

simulate growth. Capillary pressure effects in porous media are characterised by immiscible displacement saturation profiles that reflect a quadratic dependency on the saturation [31]. King and Scher [32] have extended DLA to finite-mobility ratios: saturation profiles are determined as a quadratic function of the mobility ratio in order to account for the non-zero pressure drop that is present in immiscible displacement. This pressure drop varies from point to point along the interface, and growth occurs mainly at points of high pressure gradient (i.e. field) or of least resistance. Sherwood and Nittman [33] and Sherwood [34] have modelled the effect of a finite viscosity ratio on gradient-governed growth by solving Laplace's equation for each point on the interface. Both stable and unstable types of growth are seen: in particular, DLA-type aggregation is generated in the infinite mobility ratio situation. These studies did not, however, include surface tension or capillary forces in the simulations.

Following a suggestion by Kadanoff [35], Liang [36] has mimicked the effects of surface tension by letting random walkers 'evaporate' from the cluster after first contact, with a probability proportional to the pressure discontinuity at the interface. This pressure discontinuity is inversely proportional to the local radius; therefore, a given site must be visited a minimum number of times before the interface can rearrange itself.

Finally, Paterson [37] allowed for the different permeabilities encountered in heterogeneous media by changing the lattice spacing so that walkers travel at various speeds. Alternatively, one can also vary the number of required random walkers that must hit a given site.

1.2. Invasion percolation and porous media

A porous medium can be thought of as a network of sites (bodies) connected by many bonds (necks or throats). In general, the diameter of most sites is bigger than that of bonds. However, because each set of quantities follows a wide distribution, there will be some overlap and a small number of bonds will have a larger diameter than their corresponding sites. This sets the stage for the well known Haines jumps [38] that are a feature of non-wetting displacement in porous media. The probability of those jumps depends on the value of the local capillary pressure, the solid-liquid contact angle, and the bond diameter.

In drainage, the interface first invades the larger bonds. A meniscus that is situated at the narrowest sites is thus unstable, and will spontaneously 'spring back' into a larger bond, if any exists nearby. This is because the negative curvature of a non-wetting meniscus translates into a positive gradient; thus it must be opposed by a greater gradient in order for movement to occur. Conversely, imbibition displacement is spontaneous and is most likely to occur first at the smallest sites. In other words, drainage first occurs at the largest bonds because of the lower pressure drop needed to overcome the opposing capillary pressure, whereas in imbibition a higher capillary pressure will facilitate displacement. Therefore, drainage is bond controlled and imbibition is site controlled.

Displacements in porous media thus do not occur smoothly with time; rather, they evolve in a burst-like manner, as a series of discrete steps. The result of this chain of events is mathematically known as a percolation cluster. Such a cluster can be built using a given ensemble of rules, set by Monte Carlo methods. The study of percolation is not limited to mathematics: recently, the theory of percolation was used to analyse

stochastic models of galactic evolution in which supernovae promote star formation by exploding at random intervals [39]. Traditional percolation analysis of immiscible displacement in porous media [40] successfully predicts the characteristic length of a trapped area to be linearly dependent on the inverse of the capillary number; that is, more and more of the wetting phase is displaced until all of the available pore space is invaded at very high capillary numbers. However, tapering-off of the residual saturation at very low N_{ca} reveals that trapped areas are much larger than predicted [40]. This indicates there is a different process at work that is not explained by classical percolation theory. Nonetheless, this theory gives a good description [41] of the distribution and relative amount of non-wetting phase areas, especially for isolated and dead-end pores.

Yanuka *et al* [42] modelled tridimensional porous media displacements using bond-site percolation theory: sites are chosen by pseudo-random number generation. Necks develop as a result of intersections between sites. Invasion proceeds according to classical percolation, i.e. by searching for the smallest site (or number). Unfortunately, this method is very time consuming, even for a reasonably fast computer. However, the biggest drawback of simulations based on classical percolation theory is that traps are eventually invaded. Such a situation naturally occurs for gases which are compressible, as opposed to liquids which are not. Therefore, the theory must be modified to accommodate incompressible traps and for the increasing capillary pressure that is observed with increasing saturation.

This modification is now known as 'invasion' percolation. It was first introduced in 1983 by Wilkinson and Willemsen [43] and has the advantage of rendering trapped areas inaccessible to the invading fluid. This effectively lowers the two-dimensional fractal dimension to a theoretical value of 1.82, instead of 1.89 for the classical theory. Invasion-percolation cluster growth occurs dynamically along a path of least resistance [44] by choosing the smallest available random number. A similar method was proposed recently by Ramakrishnan and Wasan [45]; however, no value for the fractal dimension was given. Wilkinson [46] has studied the macroscopic consequences of pore-level percolation behaviour of two-phase immiscible displacement and found them to be consistent with the multiphase Darcy equations. He also predicted the macroscopic behaviour of relative permeabilities and of the capillary pressure curve, as well as microscopic quantities such as the fractal dimension and the cluster size distribution, even for very low capillary numbers.

Experiments on photographically etched networks of square ducts by Lenormand and Zarcone [47, 48] confirmed and generalised those studied to include viscous fingering (diffusion-limited growth) and stable displacement. Their findings were as follows: invasion percolation (capillary fingering) ($D = 1.83$) always occurs at very low capillary numbers, no matter what is the value of the viscosity ratio; displacements at high capillary numbers are either stable ($D = 2.00$) under a favourable viscosity ratio, or undergo viscous fingering ($D = 1.50$–1.70) under unfavourable conditions of viscosities. Results are shown [48] for $M = 13$ and $M = 7.6 \times 10^{-5}$, with flow rates spanning four orders of magnitude.

Lenormand [49] has elucidated the theory behind three of the basic mechanisms for non-wetting displacement in porous media: boundaries for the phenomena are calculated in terms of M and N_{ca} ($= v\mu_{NW}/\gamma$) from a porous-medium application of Darcy's and Laplace's laws for pressure drops. These boundaries are determined for each phenomenon, or 'phase', from the geometrical properties of the medium and drawn on a phase diagram where N_{ca} is plotted against the viscosity ratio, M.

The purpose of the present work is to develop a stochastic simulation algorithm that effectively simulates actual experiments without excessive computational overhead. Results will be compared with the experiments done by Lenormand and Zarcone [48] under nearly identical conditions.

2. Theory

The theoretical details underlying diffusion-limited growth [15, 20] and invasion percolation [43, 46, 49] are given elsewhere and will not be covered here. However, developments pertinent to the extension of the DLA model to finite mobilities and non-zero surface tension will be discussed, along with some aspects of invasion percolation in porous media. The determination of stable and unstable displacement phase boundaries will also be undertaken in term of M and N_{ca}.

2.1. Finite-mobility DLA

The growth process of an invading cluster follows a transport law similar to Darcy's law when diffusion represents the controlling factor. The interfacial velocity is then

$$V = -\lambda \nabla p = F/m \tag{1}$$

p being the probability, or normalised 'pressure', of finding random walkers at any given site on the interface; F, the lattice size; m, the time expressed in Monte Carlo steps per site [50]; and λ, the generic phase mobility. Rearranging (1) we obtain the equation for gradient-governed growth, which occurs spontaneously on a negative gradient:

$$-\nabla p = V/\lambda = F/(m\lambda). \tag{2}$$

Diffusion-limited growth occurs in conditions of infinite mobility ($\lambda \to \infty$) and all points on the interface experience a negligible gradient:

$$\nabla p = 0 \qquad m \geqslant 1. \tag{3}$$

Thus growth occurs at a constant rate at all points along the interface by having all walkers stick on first contact; a discrete lattice requires that the smallest walk step be equal to one, which is also the case for miscible flood. Integrating (2) for both injected (NW) and displaced (W) phases and setting the integrating constant to unity, we obtain the smallest number of steps per site needed to advance the interface from either phase. This number corresponds to a physical pressure, namely the intraphase pressure drop [49] for radial flow at any site $0 \leqslant r \leqslant R$ from the injection point:

$$\delta p_{NW} = 1 + (q\mu_{NW}\varepsilon r/\kappa a_b^2) \tag{4a}$$

$$\delta p_{W} = 1 - (q\mu_{W}\varepsilon \ln(r/R)/2\pi\kappa a_s h) \tag{4b}$$

where q is the volumetric flow rate; $\mu_{NW;W}$, the bulk phase viscosity; ε, the medium porosity; r, the radial distance; R, the breakthrough radius; κ, the absolute permeability, expressed in lattice units; h, the medium thickness, which is unity for two-dimensional systems; $\delta p_{NW;W}$, the intraphase pressure drop for either phase; and $a_{b;s}$, the average bond (site) diameter. As the viscosity ratio, $M(=\mu_{NW}/\mu_W)$, approaches zero, random walkers only hit the interface from the wetting phase and DLA-type growth occurs because of the constant flux. On the other hand, as the viscosity ratio goes to infinity,

$\delta p_{NW} \to \infty$ and becomes much greater than the opposing capillary pressure, p_c. Therefore, all bonds can be penetrated by the invading fluid and stable displacement is favoured because the growth process is governed by the pressure gradient [33, 34, 50] rather than by the value of the mobility, as is the case for diffusion-limited growth.

2.2. Capillary pressure and percolation

The effect of introducing a surface tension is to make the growing interface of the cluster more susceptible to rearrangements after first contact, provided that $\delta p_{NW;W}$ is not too high with respect to the capillary pressure. According to Kadanoff [35], a walker can walk from the point of first contact at bond b (site s) to another point on the same cluster. The sticking probability is then

$$\phi_{NW;W}(b; s) = 1 - (4\gamma \cos \theta)/(\delta p_{NW;W} a_{b;s}) \tag{5}$$

where θ is the solid–liquid contact angle given by Young's equation; thus, non-wetting phase contacts are bond controlled, while wetting phase contacts are site controlled. Consequently, when $p_c \simeq \delta p_{NW;W}$, walkers will tend to avoid narrow bonds (sites), as has been observed for non-wetting displacement. Alternatively, when $\delta p_{NW;W} \to \infty$, the sticking probability goes to unity and we obtain the limit of vanishing surface tension. Similar relationships were derived by Liang [36] and Lenormand [49]. The probability that a wetting phase walker will 'evaporate' from the interface is

$$\Gamma_W(s) = 1 - \phi_W(s) \tag{6a}$$

whereas the sticking probability for a non-wetting phase walker is

$$\Gamma_{NW}(b) = \phi_{NW}(b) \tag{6b}$$

so that near the percolation threshold, for a square lattice,

$$\Gamma_W(s) \simeq 0.6 \tag{7}$$

for any bond–site pair [44]. The quantity $(1 - \Gamma_{NW}(b))$ corresponds to the likelihood of inactive bonds, and $\Gamma_{NW}(b)$ is the probability that a cluster site will percolate into neighbouring bond–site pairs by using open bonds. At the percolation threshold, $\Gamma_{NW}(b)$ is approximately 0.5: in classical percolation, this is the point beyond which a cluster can grow indefinitely and, appropriately, 'infect' the whole population. The fractal dimension at the invasion percolation threshold has been consistently measured by many authors [43, 44, 46, 47] to be equal to 1.82: at this point, the cluster grows very slowly. Above the classical percolation threshold, there are no limits on cluster size; below this critical value, however, growth eventually grinds to a halt, and the 'epidemic' remains confined to a small section of the population [39]. This restriction does not apply to invasion percolation, in which a cluster will continue to grow dynamically along a path of least resistance. This may also happen at the threshold when the proportion of Haines jumps is not negligible. The maximum probability of active-bond Haines jumps at the threshold is approximately 25%; that is, if the bond size distribution completely overlaps the pore (site) size distribution. In most practical cases, however, the proportion of Haines jumps remains small because there is little overlap between the two distributions, as figure 1 demonstrates. Following [39], the probability $f(x)$ of having k open bonds, or 'live' neighbours, in a four-neighbour geometry is

$$f(4) = \binom{4}{k} \Gamma_{NW}(b)^k (1 - \Gamma_{NW}(b))^{4-k} \tag{8}$$

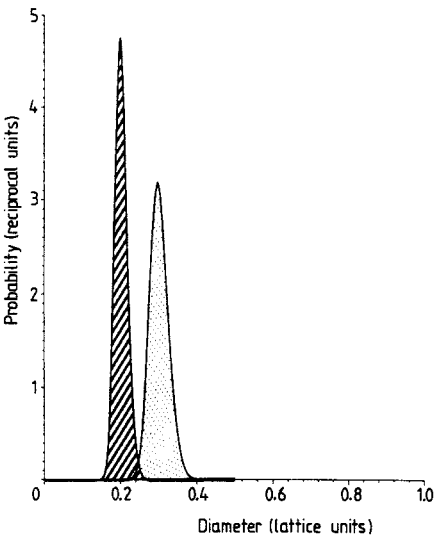

Figure 1. Bond- and pore-size log-normal distributions for bonds (hatched) and sites (dotted).

where $k = 0, 1, \ldots, 4$. A number k for each site is generated by performing four coin-toss trials per site. A similar method was used by Schulmann and Seiden [39] in galactic evolution models to obtain the number of probable infant stars born in the wake of exploding supernovae.

2.3. *Phase boundary relationships*

We now proceed to derive radial flow phase relationships similar to those given by Lenormand [49] for linear flow.

2.3.1. Limiting conditions for DLA. Combining (6*a*) and (6*b*) into a ratio proportional to $M(\approx(\delta p_{NW} a_b)/(\delta p_W a_s))$,

$$M \propto [\Gamma_W(s)/(1-\Gamma_{NW}(b))] = (1-\phi_W(s))/(1-\phi_{NW}(b)) \to 0 \tag{9a}$$

in the DLA limit. Substitution of the results in (5) gives

$$(4\gamma \cos\theta)/(\delta p_W a_s) \to 0. \tag{9b}$$

Rearranging, we get for $\delta p_W \to \infty$, using (4*b*), $\kappa \simeq a_s^2$, and $V \simeq q/a_s^2$:

$$N_{ca} \geq 4C(R/r, \theta)M \tag{9c}$$

where $C(R/r, \theta)$ is a geometrical constant $(=(2\pi \cos\theta)/\varepsilon \ln(R/r))$, which corresponds to the linear-flow constant $(=a_b/\varepsilon L)$. Except for the constant due to radial flow, (9*c*) is very similar to (8) in [49], even though the derivation is performed differently.

2.3.2. Plug-flow limit. For stable displacement we have

$$M \propto [\Gamma_W(s)/(1-\Gamma_{NW}(b))] \to \infty \tag{10a}$$

so that

$$(4\gamma \cos\theta)/(\delta p_{NW} a_b) \to 0. \tag{10b}$$

Proceeding in the same way as for (9*c*) and accounting for radial flow, we obtain

$$N_{ca} \geqslant (a_b \cos\theta)/\varepsilon(R; r). \tag{10c}$$

Thus, neutral wettability displacements would not exhibit the invasion percolation stage, even for very low N_{ca}. For linear flow (49) and $\cos\theta \simeq 1$, one obtains $N_{ca} \geqslant (a_b/\varepsilon L)$, where L is the extent of the medium. Taking the definition of M in (9*a*), we see that stable, non-wetting displacement occurs when M is greater than the ratio (a_s/a_b): a higher pressure is required from the non-wetting phase in order to compensate for the greater magnitude of the capillary pressure present in the smaller bonds.

2.3.3. Invasion percolation. From (7) and (10*a*) we obtain the sticking probabilities for invasion percolation:

$$\Gamma_{NW}(b)/(1-\Gamma_W(s)) \simeq O(1). \tag{11}$$

The interface is being hit by walkers from both phases because capillary forces are of the same order of magnitude as viscous forces. Boundaries should follow the same laws as in (9*c*) and (10*c*), but with a constant scaling factor [49] to account for the difference between microscopic (i.e. pore-scale) and macroscopic distances. Our results are thus consistent with those in [49], except that boundaries are dependent on the radial distance, r, because of the different velocity field. Nonetheless, a similar phase diagram is obtained.

Details on how the simulations were carried out will be given in the following section.

3. Methods

A square network of 65 536 capillary elements, each having a different square cross section and similar to one presented in [51], is built using a log-normal distribution centred around 0.3 lattice units (figure 1). Both permeability and porosity are determined from geometrical considerations: for example, the permeability is proportional to the square of the average bond diameter, a_b. Each capillary element consists of a site of diameter a_s, the access to which is controlled by a bond of diameter a_b. The average bond diameter, a_b, for the present work is equal to $0.75a_s$.

'Polya drunks' (i.e. random walkers) are launched either from a growing circle situated at a minimum of six lattice units ahead of the advancing interface [17] and centred on the point of injection, or launched from the latter. The frequency at which either source is chosen is determined by a binary weighted-coin toss of which the probability depends on the normalised pressure drop of the wetting fluid taken over one lattice unit. Since a lattice unit is much smaller than the breakthrough radius, R, the pressure drop over this lattice unit is well described by Darcy's law for linear flow; therefore, random walkers come from the wetting phase with a probability equal to $\bar{v}\bar{\mu}_w$, where $\bar{v}$ is the normalised velocity and $\bar{\mu}_w$ the normalised viscosity of the wetting phase. This velocity can be calculated using the phase boundary conditions given in (9*c*) and (10*c*). However, we use the more precise derivations of [49] to predict the value of the percolation threshold (equations (6) and (7) therein) and to obtain the ratio of N_{ca} to the RHS of either (8) for DLA, or (10) therein for stable displacement

[49]. The velocity is set to infinity when capillary forces are negligible with respect to viscous forces, using a scaling factor proportional to the range of capillary numbers found between the percolation threshold and the corresponding value for either plug flow or DLA. Walkers are usually allowed to walk in randomly-selected directions (chosen by permutation of indices) until they reach a nearest-neighbour site and stick to the interface with a probability $\phi_{NW;W}(b; s)$ (equation (5)). They may also stick to a next-nearest neighbour site with a probability $\phi_{NW;W}(b; s)(1-\phi_{NW;W}(b;s))^2$. Walkers which venture beyond a radius three times that of the launching circle are killed [17].

High-pressure drop conditions at velocities higher than a phase boundary are simulated by having a site visited at least m times (equation (4)) before allowing the interface to move at this point. As for the intermediate zone between the DLA and the plug-flow phase, we assume that viscous forces become predominant as N_{ca} goes to unity. Large-scale lattice effects are prevented by permitting movement in both axial and diagonal directions, with the axial one being preferred about 70% (cos 45°) of the time, because of the shorter travel distance.

Walkers diffusing from the origin are 'infected' with a disease called 'percolitis' [39] with which they can invade neighbouring cells. The probability of infection is given by (8): four coin-toss trials are performed using a weighted coin. The tally of heads determines the number of active bonds at a particular site. Trapped wetting phase areas are deemed to be 'immune' to the disease. Because only infected individuals living near the growing interface are contagious, there is a trapping rule that prevents infectious cells surrounded by a minimum of three immune cells in any direction from transmitting the disease. A record is kept of infected, but not yet contagious, individuals, so that percolation will occur every time a walker sticks to the interface from the displacing phase.

Therefore, in the stable displacement limit, $M \to \infty$ and contagion ripples through the network in concentric waves. The probability of being infected is a certainty because capillary forces are negligible and infection occurs on first contact. At high flow rates, however, percolation tends to occur in a radial direction, rather than along a direction chosen at random, because of the stronger pressure drop experienced by radially oriented pores. On the other hand, walkers hitting from the displaced phase cannot percolate because they represent disruptive processes which are involved in unstable displacement. Conditions for which capillary forces are negligible are simulated by applying phase boundary conditions to the ratio, $(4\gamma \cos\theta)/(\delta p_{NW;W} a_{b;s})$, which is then normalised to probabilities using the transformation $x \to x/(1+x)$.

This process is continued until a preset breakthrough radius is reached by the cluster. Recovery is estimated by calculating the respective areas of empty and filled capillary elements within the breakthrough radius.

The fractal dimension, D, is determined as a function of the non-wetting saturation

$$S_{NW} \propto r^{(D-2)}. \tag{12}$$

Given that $S_{NW} = N/r^2$, where N is the number of lattice units invaded by the displacing fluid, (12) yields $N \propto r^D$, D being the log-log slope of N against r [43]. The method used in this work is described by Forrest and Witten [14]. Growth beyond the radius of gyration is still incomplete and, therefore, determination of the fractal dimension is not carried out over distances 20% beyond the radius of gyration.

All programming was done in FORTRAN 77. Extensive use was made of IMSL (Houston, TX, USA) library routines, in particular GGUBFS (pseudo-random number

generator), GGPER (random permutations), GGBN (binomial distribution; weighted-coin tosses) and GGNLG (log-normal distribution).

Simulations were performed using the VM/SP 370 CMS and VMBATCH environments on the University of Ottawa Computing Centre's AMDAHL 470 V8 computer. The simulation parameters (see table 1) represent conditions very similar to those present in the experiments carried out by Lenormand and Zarcone [48].

Table 1. Results of numerical experiments.

Figure	M	N_{ca}	D	Γ_{NW}	% recovery
2(*a*)	7.6×10^{-5}	2.30×10^{-10}	1.90-1.94	0.916	78-83
2(*b*)	7.6×10^{-5}	1.15×10^{-9}	1.80-1.84	0.688	28-48
2(*c*)	7.6×10^{-5}	1.15×10^{-8}	1.80-1.84	0.172	18-26
2(*d*)	7.6×10^{-5}	1.15×10^{-7}	1.54-1.58	0.008	13-14
2(*e*)	7.6×10^{-5}	1.15×10^{-6}	1.50-1.54	0.000	14-18
3(*a*)	13	3.0×10^{-6}	1.77-1.83	0.745	35-39
3(*b*)	13	6.0×10^{-6}	1.83-1.87	0.853	35-55
3(*c*)	13	1.5×10^{-5}	1.95-1.97	0.935	78-84
3(*d*)	13	1.5×10^{-4}	1.99-2.00	0.992	96-97
3(*e*)	13	1.5×10^{-2}	1.99-2.00	0.997	97-98

4. Results and discussion

A network of pores and sites was generated using a log-normal distribution, as described in the preceding section. Figure 1 shows a graph of each distribution in terms of lattice units. Before performing the second set of simulations ($M = 13$, $\theta = 50°$), the percolation probability, $\Gamma_{NW}(b)$, was weighted with a constant (≈ 2.05) until the percolation threshold was reached. This was done at the predicted threshold value for favourable displacement ($N_{ca} = 1.5\times10^{-6}$). A fractal dimension consistent with invasion percolation was also measured with a weighting factor of 1.15 when conditions were changed to $N_{ca} = 1.75\times10^{-9}$, $M = 7.6\times10^{-5}$ and $\theta = 70°$: the percolation probability for these conditions was found to be approximately 0.5. Small differences with the results given in [49] may be accounted for by slightly different porosities, permeabilities and uncertainties in the contact angle measurements given in [49].

Simulations were performed five times for each set of conditions (table 1), except for the longer runs near the percolation threshold. Results were averaged and are tabulated in table 1. Sample runs are shown in figure 2(*a-e*) for $M = 7.6\times10^{-5}$, and in figure 3(*a-e*) for $M = 13$. Experiments 2(*b*) and 3(*a*) were run near the percolation threshold. The lowest recoveries are observed for DLA (figure 2(*d*)), and are quite close to the predicted value of 11% [24]. Fractal dimensions are lower than predicted, possibly because of some screening effects in the growth process [24]: the biggest fingers act as traps and stunt the growth of smaller fingers. Increasing the interface velocity is equivalent to having either a higher intrafluid pressure drop or a lower mobility, which both have the effect of further stabilising the interface by smoothing out noise [50] over m walk steps (Equation (4)), before the meniscus can advance. Fatter, dendritic fingers result (figure 2(*e*)) from a slightly gradient-controlled process

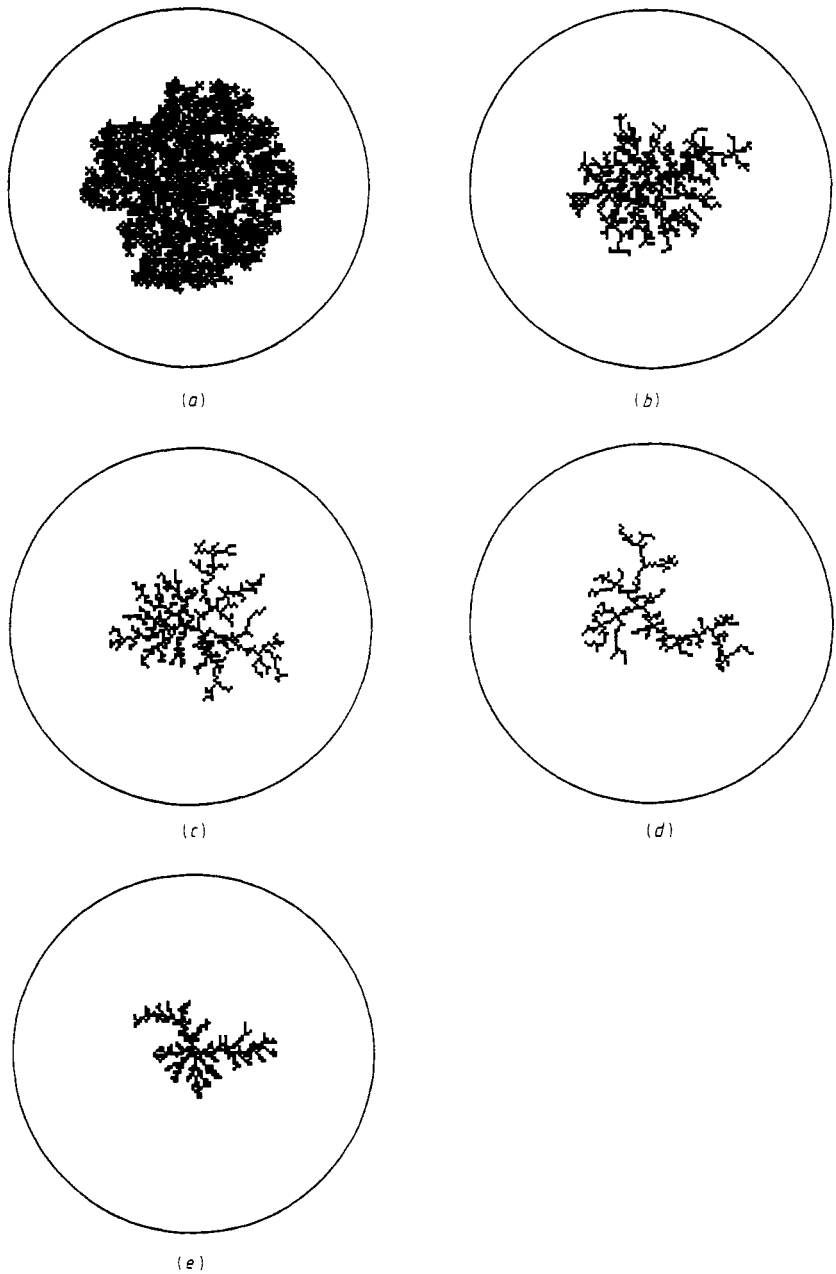

Figure 2. Sample numerical experiments for $M = 7.6 \times 10^{-5}$, $\theta = 70°$; $\gamma = 66\ \mathrm{mN\ m^{-1}}$; $\varepsilon = 0.13$; $\kappa = 0.04$. (*a*) $N_{ca} = 2.30 \times 10^{-10}$; (*b*) $N_{ca} = 1.15 \times 10^{-9}$; (*c*) $N_{ca} = 1.15 \times 10^{-8}$; (*d*) $N_{ca} = 1.15 \times 10^{-7}$; (*e*) $N_{ca} = 1.15 \times 10^{-6}$.

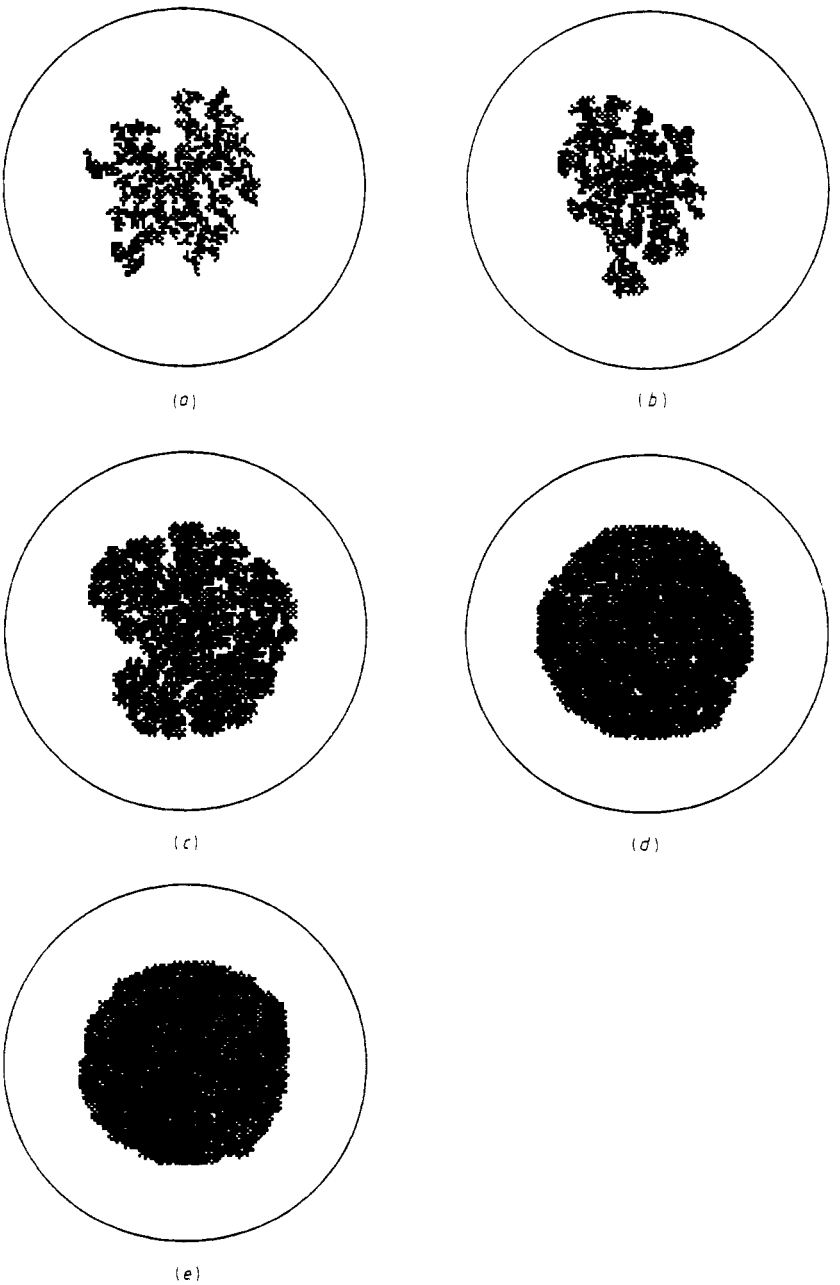

Figure 3. Sample numerical experiments for $M = 13$, $\theta = 50°$; $\gamma = 18\ \mathrm{mN\ m^{-1}}$; $\varepsilon = 0.13$; $\kappa = 0.04$. (*a*) $N_{ca} = 3.0 \times 10^{-6}$; (*b*) $N_{ca} = 6.0 \times 10^{-6}$; (*c*) $N_{ca} = 1.5 \times 10^{-5}$; (*d*) $N_{ca} = 1.5 \times 10^{-4}$; (*e*) $N_{ca} = 1.5 \times 10^{-2}$.

and, although the fractal dimension is much lower (table 1), recoveries are slightly higher than for DLA. This type of finger is also seen in [48] for $N_{ca} = 1.15 \times 10^{-6}$ and $M = 7.6 \times 10^{-5}$. Dendritic growth may also explain the slight increase in recovery seen in [10] for very high flow rates; recovery undergoes a steep decrease when passing from the invasion percolation threshold to the diffusion-limited stage, where recovery reaches a minimum. At the present time, it is not yet clear [50] whether dendritic growth represents a special, noiseless case of DLA or forms a very different type of process. The low values for the fractal dimension indicate that the second alternative may apply.

Recoveries for invasion percolation are in the 25–50% range; this indicates that low flow rate oil displacement may be called for in order to effect higher breakthrough recoveries, especially when dealing with heavy crude oils. These and the remainder of the experiments show displacement patterns and recoveries that are consistent with those obtained in [48].

The level of agreement with previous experimental work [27, 29, 36, 47, 48] is remarkable, considering the range of viscosities, surface tensions, and flow rates over which simulations were performed. Our results for very low N_{ca} confirm the invasion percolation experiments by Lenormand and Zarcone [47, 48]. With the algorithm presented here, we have observed viscous fingering fractals for about the same conditions as in [27, 29, 36, 48]. Stable displacement, on the other hand, is observed in similar conditions by King and Scher [32], by Sherwood [34] and by Lenormand and Zarcone [48].

The simulation method described in the present work can therefore address both stable and unstable types of displacement in porous media, from diffusion-limited aggregation to invasion percolation and plug flow.

Work is in progress for simulating conditions closer to those observed in actual reservoir displacement situations including: complex pore size distributions; local variations in wettability; regions of different permeabilities; and the determination of boundaries for dendritic growth.

5. Summary

A predictive algorithm for simulating non-wetting, immiscible displacement in porous media is described in terms of viscosity ratio and capillary number. Invasion percolation, viscous fingering and plus flow are identified as distinct behaviours resulting from the interplay of capillary and viscous forces.

Simulation of these phenomena is achieved by letting two kinds of random walkers hit an interface with a frequency ratio proportional to the viscosity ratio, and stick to that interface with a probability inversely proportional to the interfacial tension. In addition, walkers diffusing from the displacing phase are subject to a percolation mechanism similar to the propagation of epidemics and which follows a biased binomial distribution generated by the sticking probability. For example, all neighbours will be invaded (i.e. infected) if capillary forces are much less important than viscous forces, and recovery will tend to be complete. On the other hand, viscous fingering is observed for high flow rates and very low viscosity ratios. Finally, invasion percolation ($D = 1.82$) is the sole displacement mechanism at low capillary numbers: for example, at the predicted precolation threshold, the sticking probability for the non-wetting phase is observed to be equal to approximately 0.5 for a viscosity ratio of 7.6×10^{-5}. Results

are compared with previously reported experiments and are found to be in good agreement with respect to recovery and growth rate exponent.

Acknowledgment

Financial support from the Natural Sciences and Engineering Research Council of Canada is gratefully acknowledged.

References

[1] Witten T A and Cates M E 1986 *Science* **232** 1608
[2] Homsy G M 1987 *Ann. Rev. Fluid Mech.* **19** 271
[3] Saffman P J and Taylor G I 1958 *Proc. R. Soc.* A **245** 312
[4] Chuoke R L, Van Meurs P and Van Der Poel C 1959 *Trans. Am. Inst. Min. Engng.* **216** 188
[5] Peters E J and Flock D L 1981 *Soc. Pet. Engng. J.* **21** 249
[6] McLean J W and Saffman P G 1981 *J. Fluid Mech.* **102** 455
[7] Tryggvason G and Aref H 1983 *J. Fluid Mech.* **136** 1
[8] De Gregoria A J and Schwartz L 1986 *J. Fluid Mech.* **164** 383
[9] Paterson L 1981 *J. Fluid Mech.* **113** 513
[10] Ni L W, Hornof V and Neale G 1986 *Rev. Inst. Fr. Pet.* **41** 217
[11] Stokes J P, Weitz D A, Gollub J P, Dougherty A, Robbins M D, Chaikin P M and Lindsay H M 1986 *Phys. Rev. Lett.* **57** 1718
[12] Mohanty K K, Davis H T and Scriven L E 1987 *SPE Reservoir Engng.* **2** 113
[13] Mullins W W and Sekerka R F 1963 *J. Appl. Phys.* **34** 323
[14] Forrest S R and Witten T A 1979 *J. Phys. A: Math. Gen.* **12** L109
[15] Witten T A and Sander L M 1981 *Phys. Rev. Lett.* **47** 1400
[16] Witten T A and Sander L M 1983 *Phys. Rev.* B **27** 5686
[17] Meakin P 1983 *Phys. Rev.* A **27** 604, 1495
[18] Turkevitch L A and Scher H 1985 *Phys. Rev. Lett.* **55** 1026
[19] Matsuhita M, Sand M, Hayakawa Y, Honjo H and Sawada Y 1984 *Phys. Rev. Lett.* **53** 286
[20] Niemeyer L, Pietronero L and Wiesmann H J 1984 *Phys. Rev. Lett.* **52** 1033
[21] Weitz D A and Oliveria M 1984 *Phys. Rev. Lett.* **52** 1433
[22] Meakin P 1983 *Phys. Rev. Lett.* **51** 1119
[23] Kolb M, Botet R and Jullien R 1983 *Phys. Rev. Lett.* **51** 1123
[24] Paterson L 1984 *Phys. Rev. Lett.* **52** 1621
[25] Nittman J, Daccord G and Stanley H 1985 *Nature* **314** 141
[26] Daccord G, Nittman J and Stanley H 1986 *Phys. Rev. Lett.* **56** 336
[27] Maloy K J, Feder J and Jossang T 1985 *Phys. Rev. Lett.* **55** 2688
[28] Chan D Y C, Hughes B D and Paterson L 1986 *Phys. Rev.* A **34** 4079
[29] Chen J D and Wilkinson D 1985 *Phys. Rev. Lett.* **55** 1892
[30] De Gregoria A J 1985 *Phys. Fluids* **28** 2933
[31] Allen F R and Pickett D R 1986 *SPE Prod. Engng.* **1** 62
[32] King M J and Scher H 1987 *Phys. Rev.* A **35** 929
[33] Sherwood J D and Nittman J 1986 *J. Physique* **47** 15
[34] Sherwood J D 1986 *J. Phys. A: Math. Gen.* **19** 1195
[35] Kadanoff L P 1985 *J. Stat. Phys.* **39** 267
[36] Liang S 1986 *Phys. Rev.* A **33** 2663
[37] Paterson L 1987 *J. Phys. A: Math. Gen.* **20** 2179
[38] Haines H B 1930 *J. Agric. Sci.* **20** 97
[39] Schulman L S and Seiden P E 1986 *Science* **233** 425; 1978 *J. Stat. Phys.* **19** 293; 1982 *J. Stat. Phys.* **27** 83
[40] Larson R G, Scriven L E and Davis H T 1977 *Nature* **268** 409
[41] Larson R G, Scriven L E and Davis H T 1981 *Chem. Engng. Sci.* **36** 57
[42] Yanuka M, Dullien F A L and Elrick D E 1986 *J. Colloid Interface Sci.* **112** 24

[43] Wilkinson D and Willemsen J 1983 *J. Phys. A: Math. Gen.* **16** 3365
[44] Wilkinson D and Barsony M 1984 *J. Phys. A: Math. Gen.* **17** L129
[45] Ramakrisnan T S and Wasan D T 1986 *Int. J. Multiphase Flow* **12** 357
[46] Wilkinson D 1986 *Phys. Rev.* A **34** 1380
[47] Lenormand R and Zarcone C 1985 *Phys. Rev. Lett.* **54** 2226
[48] Lenormand R and Zarcone C 1985 *PhysicoChem. Hydrodyn.* **6** 497
[49] Lenormand R 1985 *C.R. Acad. Sci., Paris* **301** 247
[50] Szep J, Cserti J and Kertesz J 1985 *J. Phys. A: Math. Gen.* **18** L413
[51] Dullien F A L 1975 *AIChE J.* **21** 299